J. Min. Metall. Sect. B-Metall. 61 (3) (2025) 293 - 302

Journal of Mining and Metallurgy, Section B: Metallurgy

EFFECTS OF WELDING PARAMETERS ON PERCENTAGE DILUTION AND MECHANICAL PROPERTIES IN WELDED JOINTS OF ULTRA-HIGH HARDNESS ARMOUR STEELS

Charles Hudson Martins de Vasconcelos [a,c*], Naiara Vieira Le Sénéchal [a], Cristhian Ricardo Loayza Loayza [b], Ademir Ângelo Castro Filho [b], Eduardo de Magalhães Braga [b], Andersan dos Santos Paula [a], Ricardo Pondé Weber [a]

[a] Military Institute of Engineering - IME, Graduate Program in Materials Science and Engineering, Rio de Janeiro, RJ, Brazil

[b] Federal University of Para - UFPA, Department of Mechanical Engineering, Belem, PA, Brazil

[c] Instruction Center Almirante Braz de Aguiar - CIABA, Belem, PA, Brazil

(Received 11 December 2023; Accepted 06 November 2025)

Abstract

This study investigates the effects of Gas Metal Arc Welding (GMAW) parameters—specifically welding speed and stick-out—on the dilution and mechanical properties of welded joints composed of ultra-high hardness quenched and tempered (UHH-Q&T) armor steel and austenitic stainless steel filler metal. An optimization methodology was used to set constant parameters, including wire diameter, gas flow rate, welding voltage, and wire feed speed, based on equipment capabilities. Experimental trials varied welding speed and electrode stick-out while maintaining a constant current through inductance control. Although the welding parameters affected the melted base and filler metal areas, the dilution percentage remained unaffected. The correlation between dilution and welding current was validated. Microstructural and mechanical analyses confirmed the consistent behavior of the welded joints under the tested conditions.

Keywords: *Ultra-high hardness steel; GMAW; Dilution; Heat-affected zone; Mechanical properties*

1. Introduction

In recent decades, research in the field of armor has primarily focused on developing lightweight armor technologies capable of defeating Armor Piercing (AP) projectiles. To meet these demands, the availability of quenched and tempered armor steels has expanded, most notably through the updated MIL-DTL-46100E specification for High Hardness Armor (HHA) steels [1]. While this metallic specification has fulfilled its intended applications, substantial progress has been made in the development of Ultra-High Hardness Quenched and Tempered (UHH-Q&T) monolithic steels, with hardness levels exceeding 600 HB. These advancements have reinforced the relationship between increased steel hardness and enhanced ballistic resistance [2].

Despite the widespread application of UHH steels in ballistic protection systems, there is a noticeable lack of studies correlating dilution behavior with microstructural evolution in welded joints involving these alloys. In particular, few works analyze how dilution percentages affect the formation of specific transformation zones, such as softened intercritical HAZ regions, and their compliance with military performance criteria. This study addresses that gap by investigating the influence of GMAW parameters on dilution and related mechanical properties.

Fusion welding is one of the most widely used joining techniques in shielding projects. However, welded joints represent critical areas, as welding alters the microstructure and properties of the material, primarily due to peak temperatures surpassing the material's characteristic critical temperature [3]. During fusion welding, numerous tests and adjustments are required to identify optimal process parameters and assess their impact on product quality. The quality of the welded joint can be defined by several characteristics, with dilution being one of the most significant. The geometry of the weld bead, which influences dilution, plays a crucial role in determining the mechanical properties of the weld. Controlling the amount of base metal (BM) in the formation of the welded joint is essential, especially in applications such as welding dissimilar metals, welding coatings, and joining a BM with an unknown composition or high levels of impurities or elements detrimental to the weld [4–7]. Achieving the desired

Corresponding author: charles.vasconcellos@ime.eb.br

https://doi.org/10.2298/JMMB231211023V

dilution requires precise control over the relevant process parameters to ensure the appropriate bead shape and geometry, which ultimately determines the welding capability.

Zhang et al. [8] conducted a chemical composition analysis to compare dilution values achieved using various methods and explored the impact of heat inputs on solder dilution. The results indicated that the proposed mathematical model and the definition of welding dilution were in good agreement. Notably, the study observed that the weld could become more concentrated when the filler wire shared a similar composition to the base material, especially as the dilution of the weld exceeded a critical value. Additionally, the technique demonstrated that the overall dilution of a weld bead is a combined result, influenced by each individual composition.

Similarly, in their experimental study, Lin et al. [9] defined weld dilution as the alteration in the chemical composition of the weld metal caused by the melting of the BM component, which contributes to the formation of the fusion zone (FZ). The measurement of dilution is determined by the proportion of BM that contributes to the formation of the weld fillet, and this varies depending on factors such as joint type, preheating temperature, consumables, and welding parameters, among other conditions. The performance of welded materials is solution-dependent in many applications, and as a result, significant failures can often be attributed to this factor.

Nweze and Achebo [10] applied the TIG welding process to produce weld samples, subsequently inputting percentage dilution measurements into a fuzzy logic program. Voltage, current, gas flow rate, and welding speed were considered as process parameters.

Previous studies [11-12] have investigated dilution in fusion welding processes of metallic materials. However, no research has addressed ultra-high hardness steels. This work aims to evaluate the effect of Gas Metal Arc Welding (GMAW) parameters on the dilution coefficient in welded joints of UHH-Q&T shielding steel. Additionally, the microstructural characterization and mechanical properties of the welded joints are analyzed.

2. Experimental procedures

2.1. Materials

The material used for this study was UHH-Q&T steel, nominal composition 0.47C - 1.0Mn - 0.7Si - 3.0Ni - 1.5Cr - 0.7Mo (wt. %), class 1500 MPa yield limit, with Low-Temperature-Tempering (LTT), thickness 5 mm, classified as shielding level. Mechanical properties of material are shown in Table 1.

The selection of filler materials was based on results reported in previous literature [13-17], manufacturers' specifications [18-20], and the welding requirements for armor steel in accordance with MIL-STD 1185 standards [21]. The use of austenitic filler metal is advantageous in reducing the susceptibility to cold cracking [15, 17]. To minimize the deterioration of the heat-affected zone (HAZ) microstructure due to softening, the welder applied the lowest possible filler wire welding current [14-16, 22-23]. Consequently, the austenitic stainless steel (ASS) filler metal selected for the welding process was solid wire of class ER307, with a diameter of 1.2 mm, in compliance with the ASME SFA-5.9 classification [24].

2.2. Methods

The BM used in all stages of this study was extracted from sheets of the investigated material with dimensions of 500 × 500 × 5 mm. Specimens were cut using the wire electrical discharge machining (WEDM) process. The sections of the specimens were initially prepared by continuous sanding, followed by electrolytic polishing with 20% perchloric acid, and subsequently etched with a 2% nital reagent. Microstructural analyses of the BM were performed using optical microscopy (OM), scanning electron microscopy (SEM), and electron backscatter diffraction (EBSD) on the specimen section containing the thickness plane.

Weldability of the BM: The influence of alloying elements on the hardness and microstructure of the HAZ in structural steels, as well as their susceptibility to hydrogen-induced cracking (HIC) and the determination of preheating temperatures, is often evaluated through the equivalent effect of carbon. This assessment is expressed by equations known as the "carbon equivalent" (CE). Several CE equations are reported in the literature, developed for different applications and ranges of steel chemical compositions. The most widely recognized expression, adopted by the International Institute of Welding (IIW), is [25]:

$$CE_{IIW} = C + \frac{Mn}{6} + \frac{Cr + Mo + V}{5} + \frac{Cu + Ni}{15} \quad (1)$$

Preliminary Welding Tests: A series of preliminary welding tests was conducted using an optimization methodology that combined the Taguchi method with Gray Relational Analysis (GRA) under extreme welding conditions. These tests identified that the parameters of wire diameter, shielding gas flow rate, welding voltage, and electrode wire feeding speed (Table 1) would remain constant during the subsequent welding trials. Among these, the electrode wire feeding speed is particularly critical, as the

welding current in the selected equipment model is primarily dependent on this parameter. The welding tests were performed using a Digiplus A7 electronic source, which features an automatic current self-adjustment system and inductance control that regulates the current rise and fall rates during welding — a factor that significantly influences arc stability and spatter formation. The current obtained in the tests was classified as constant, with variations within the narrow range of 342–345 A. The optimized welding speed was set between 100 and 120 cm/min, while the stick-out distance ranged from 15 to 18 mm, as shown in Table 2.

Welding: The welding process parameters are detailed in Table 2. Tensile BM sheets with dimensions of 125 × 250 × 5 mm were joined using the semi-automatic GMAW process, without preheating, in the flat welding position (1G), with a single pass. Circular ASS wire was used as the filler metal. The sheets were machined by WEDM to form a butt joint with an "I" groove configuration and a 2.0 mm gap between them.

Dilution Measurement: The dilution coefficient (δ), or simply dilution, was determined based on the macrograph of the weld cross-section, as illustrated in Figure 1. The coefficient represents the proportion of the BM melted during welding relative to the total molten material, including both BM and filler metal. The dilution coefficient was calculated by measuring the areas corresponding to the molten BM (B) and the molten filler metal (A), according to Equation 1 [26]:

$$\delta = \frac{B}{A+B} \times 100 \quad (2)$$

The weld property characterization parameter used in this study is the dilution percentage. However, the mechanical and metallurgical properties of the weld seam and the HAZ, as well as their comparison with the base metal properties, were also of interest making use of the following methods.

Metallographic Examination of Welded Joints: Test specimens of the welded joints were extracted from the weld cross-section. For the measurement and calculation of geometric characteristics, specimens were exclusively taken from the central region of each welded plate to ensure the inclusion of the FZ, HAZ, and BM. Macroscopic analysis was performed to detect defects along the weld line and in the transverse section, with the latter also used to evaluate the geometric characteristics of the weld. The section preparation followed procedures like those applied for the BM. Macrostructural images were obtained using both a conventional digital camera and a ZEISS SteREO Discovery modular optical stereomicroscope with motorized zoom for detailed cross-sectional visualization. Microstructural analysis was carried out to obtain micrographs of the FZ-HAZ interface and the HAZ region itself, in comparison to the BM. OM was performed following ASTM E45-18a [27], while SEM was conducted according to ASTM E2142-08 [28].

Microhardness: The microhardness of the welded joint was evaluated using the Vickers microhardness test, performed with a LEITZ MINILOAD-2 device, in accordance with ASTM E384 [29], applying a load of 0.1 kgf and a dwell time of 30 seconds. Indentations were spaced at 0.1 mm intervals along three lines positioned on the upper, central, and lower surfaces across the specimen thickness, as illustrated in Figure 2. The indentations were performed on the cross-section of the welded sample, covering the

Table 1. *Main mechanical properties of UHH-Q&T*

Hardness (HBW)	Impact Toughness -40 °C (J)	Yield strength (MPa)	Tensile Strength (MPa)	Elongation (%)
570 – 640	12	1500	2000	7

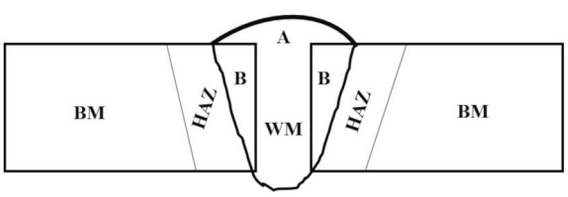

Figure 1. *Schematic of welded joint (A: Filler material cast; B: BM cast; WM: Weld metal*

Table 2. *Optimized welding conditions and parameters*

Parameters	Experiment Nº			
	1	2	3	4
Welding process	GMAW	GMAW	GMAW	GMAW
Wire diameter (mm)	1.2	1.2	1.2	1.2
Flow of gas (L/min)	19	19	19	19
Welding voltage (V)	31	31	31	31
Electrode Wire Feeding Speed (m/min)	16	16	16	16
Welding speed (cm/min)	100	100	120	120
Stick out (mm)	18	15	18	15
Current (A)	345	342	344	342

entire welded joint from one side to the other in the sequence BM-HAZ-FZ-HAZ-BM. Each line started and ended at the same distance from the weld centerline to ensure consistent measurements. The microhardness obtained was correlated with the microstructures of the BM, FZ, and HAZ to evaluate the hard distribution across the welded joint.

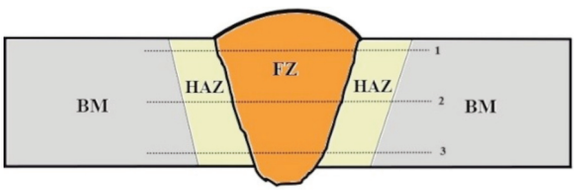

Figure 2. *Positions for observing microhardness in the welded joint: 1 - upper line, 2 - central line and 3 - lower line*

3. Results and Discussion

3.1. Microstructural characterization of the BM

The microstructural characteristics of the BM, observed through OM after etching with 2% nital reagent, reveal the presence of columnar laths and lath blocks, as shown in Figure 3, confirming that the material consists of tempered martensitic steel. No elongated inclusions were detected, which corroborates the efficiency of the liquid steel refining process and validates that the steel exhibits a cleanliness level suitable for applications with stringent requirements, particularly regarding toughness at low temperatures.

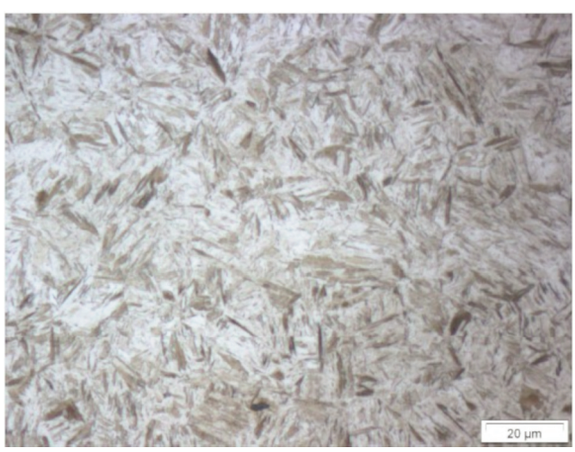

Figure 3. *Optical micrograph of BM*

Figure 4 presents a SEM image, evidencing that the laths observed in the previous image correspond to acicular-shaped martensite laths. The inverse pole figure (IPF) of UHH-Q&T steel, obtained by EBSD, is shown in Figure 5. The results corroborate microscopic observations, confirming that the steel is predominantly composed of lath-type tempered martensite, with a small fraction of retained austenite.

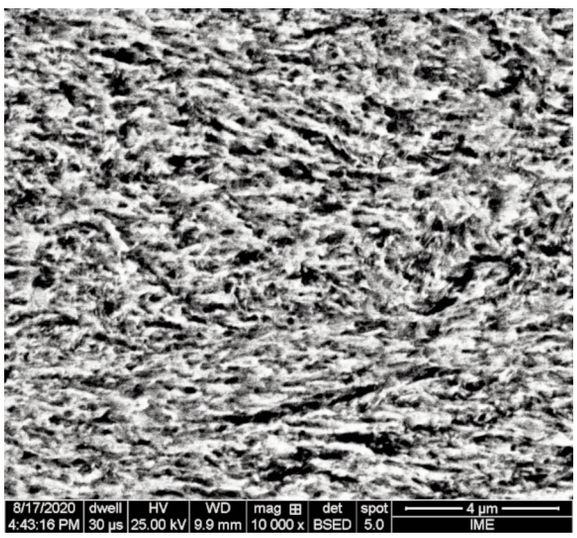

Figure 4. *SEM micrographic of BM*

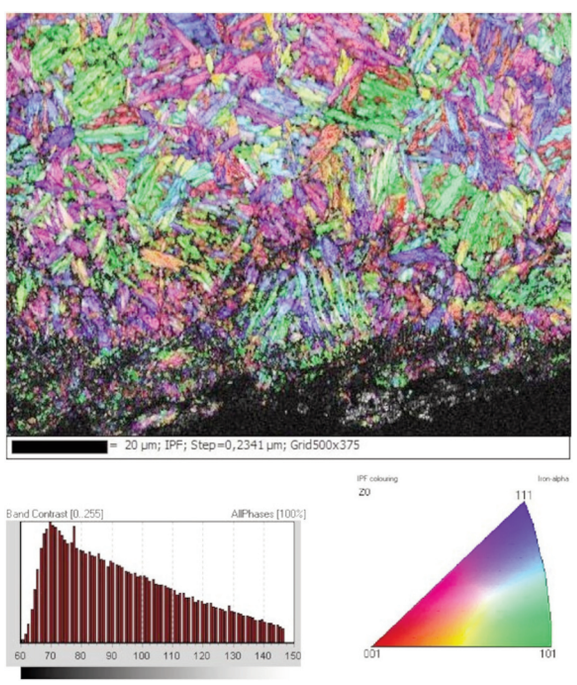

Figure 5. *Inverse pole figure of BM*

3.2. Weldability of the BM

The CEIIW value of the BM, calculated using equation 1, was 0.85%. Since this exceeds 0.80%, it is characteristic of UHH-Q&T steel intended for Class 2 shielding applications, as specified in the MIL-DTL-46100E standard [1].

3.3. Dilution coefficient

Table 3 presents the joint dilution percentages, revealing similar levels across the four experiments. It can be observed that the dilution percentage remains consistent despite variations in welding speed and stick-out parameters, with 100% of the values falling within two standard deviations, following the same trend as the welding current, as previously highlighted. This behavior aligns with the findings of Kannan and Murugan [30] for duplex stainless steel and Ohwoekevwo et al. [31] for AISI 1020 low-carbon steel, both of which reported the strongest correlation between dilution and welding current.

Dilution significantly influences the mechanical and metallurgical properties of the weld metal, as its composition deviates from the pure filler wire properties. This phenomenon can be explained using the Schaeffler diagram [12, 32]. Figure 6 illustrates the Schaeffler diagram for the four experiments, showing that the weld metal microstructure in all cases consists of austenite and martensite. The microstructural composition obtained in the four tests remains similar, despite variations in the welding parameters.

3.4. Macrostructure of welded joints

Figure 7 presents the macrographs of the welded joints obtained from processes performed with different parameters (refer to Table 2), revealing a noticeable variation in the FZ profile. All welded joints exhibit homogeneity, with no observed defects, inclusions, or cracks. Penetration is adequate, and no lack of fusion was detected in any of the samples, all of which met the acceptance criteria. Additionally, a dye penetrant test (PT) was conducted on the welded specimens.

Table 3. *Areas of the fused zone of welded joints and dilution percentage*

Exp. Nº	A (mm^2)	B (mm^2)	A + B (mm^2)	δ (%)
1	26.24	35.52	61.76	57.52
2	13.64	14.27	27.91	51.14
3	21.53	31.60	53.13	59.47
4	9.08	13.72	22.80	60.17
			Average (μ)	57.07
			Standard Deviation (σ)	± 4.11

3.5. Microstructure analysis of welded joints

A duplex microstructure consisting of fine vermicular or skeletal delta ferrite within a predominantly austenitic matrix is observed in the central region of the FZ of the welded joints (region A), as shown in Figure 8(a). The microstructure of the FZ (region B)–HAZ interface region is presented in Figure 8(b). This region, located at the interface between the ASS and UHH-Q&T materials, reveals the presence of a phase commonly referred to as the "white phase," which is characteristic of this condition and consists of highly alloyed martensite. Its formation and width are strongly influenced by the chemical composition of the filler metal. The "white" phase region and the melting boundary are in close proximity. The formation of this carbon- and chromium-rich phase in welds produced with austenitic filler metal results from the diffusion of carbon from the MB region into the filler metal region, along with the migration of chromium in the opposite direction. This process is influenced by the thermal welding cycle applied during joint fabrication [33].

Initial microstructural analyses of the welded joints indicated that the BM exhibits high hardenability. This is evidenced by the predominantly

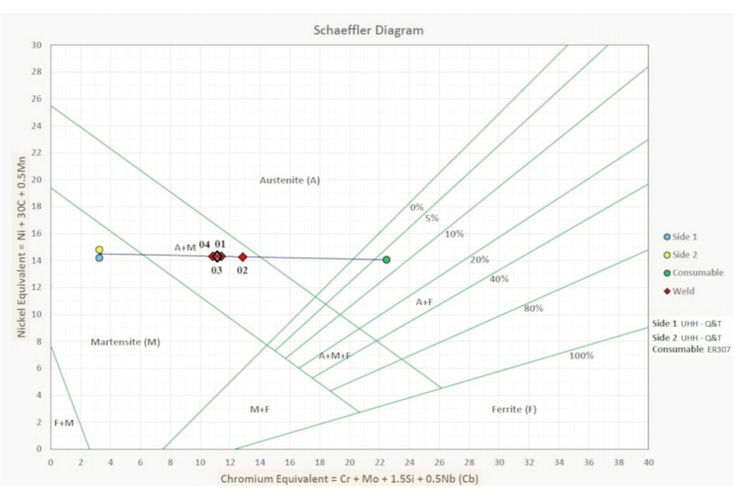

Figure 6. *Schaeffler diagram indicating the locations of filler wire (consumable), base metal (Side 1 and Side 2), and the compositions of weld metal with different joints (different dilutions)*

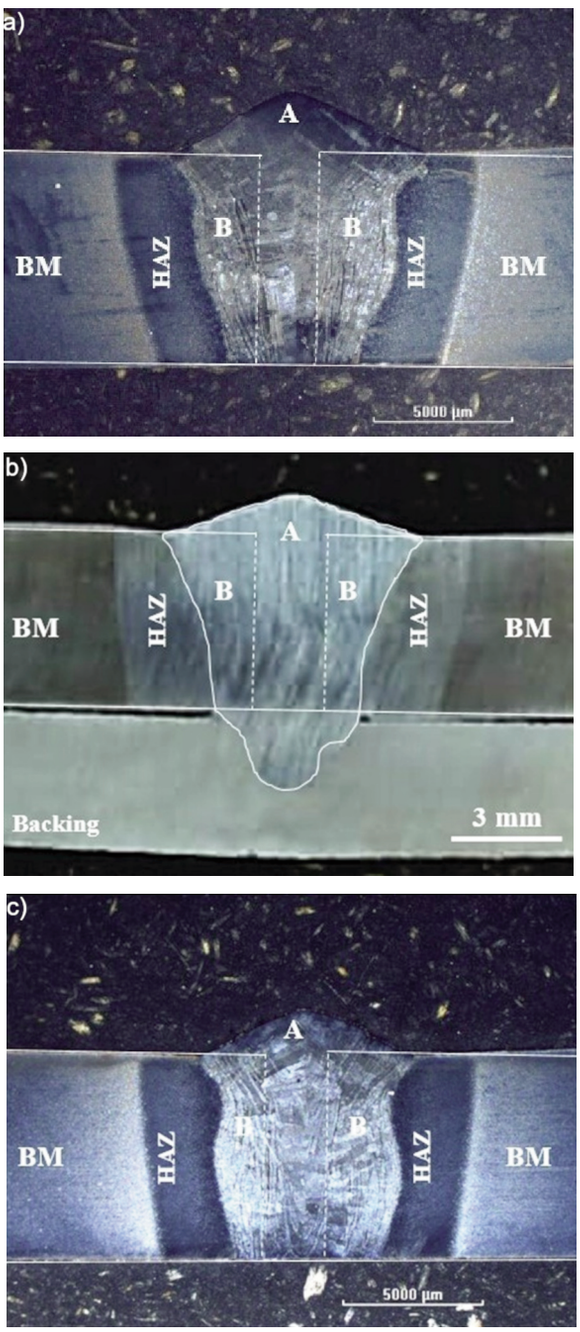

Figure 7. *Macrographs regarding: (a) experiment 01; (b) experiment 02 and (c) experiment 03*

martensitic microstructure observed across most of the HAZ extension, which closely resembles that of the BM. As shown in Figure 9, minor variations in martensitic microstructural features are observed along the HAZ, likely associated with differences in thermal input during the welding process, leading to the formation of subzones, albeit with limited dimensions. The presence or absence of tempered martensite in this region can be confirmed through

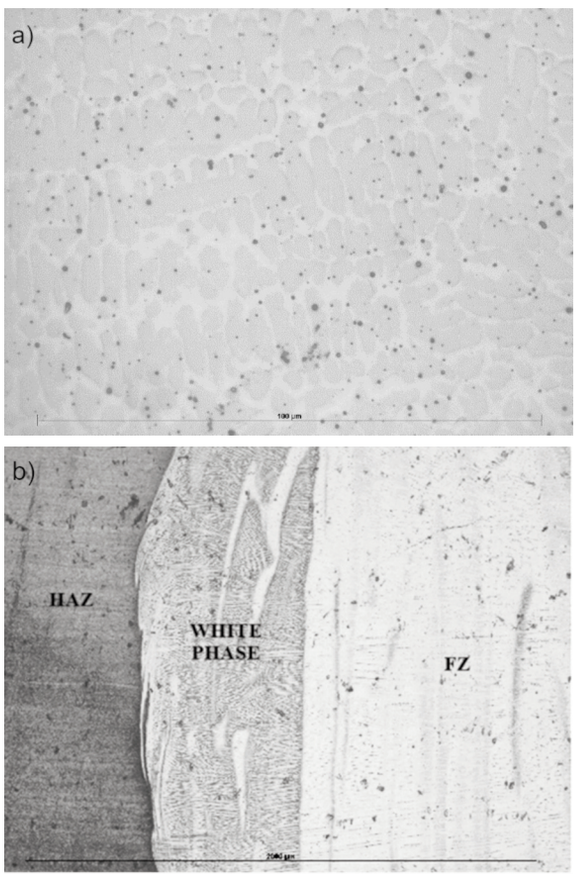

Figure 8. *(a) Microscopy via OM revealing duplex microstructures of vermicular delta ferrite in a simple austenitic matrix in the FZ region; (b) FZ-HAZ interface after etching*

hardness measurements, enabling the construction of the welded joint's hardness profile.

3.6. Microstructure and microhardness relation

The hardness profile of the welded joint, determined by the Vickers microhardness test, is shown in Figure 9, revealing significant variations in hardness across the joint. The FZ exhibited the lowest hardness values (351 HV), characteristic of austenitic steels, making this region the softest within the welded joint.

The selection of filler metals should consider both the strength and tough requirements of the joint, along with the prevailing restraint conditions. To achieve an optimal balance between strength and toughness, the filler metal with the lowest possible strength that still satisfies the joint's strength requirements should be selected, while overmatching should be avoided. Whenever possible, welds should be positioned in low-stress regions, where the use of undermatching consumables is typically viable. Lower-strength consumables offer several advantages over higher-

strength alternatives, including greater plastic deformation capacity (ductility), reduced susceptibility to cracking, and improved toughness in the welded joint [13].

The hardness survey also encompassed the HAZ, from which four distinct subzones were identified. The subzone closest to the FZ, corresponding to the CGHAZ, exhibited the highest hardness values, ranging from 675 to 730 HV, attributed to the formation of martensite. Moving towards BM, the hardness remains elevated, with an average value of 690 HV. This region is associated with the FGHAZ, where the peak temperature, although exceeding the Ac3 transformation temperature, is lower than that reached in the CGHAZ. Adjacent to the FGHAZ, the ICHAZ is characterized by an abrupt drop in hardness, likely due to the welding thermal cycle inducing partial austenitization of the material. Further towards the BM, the hardness gradually increases until reaching the BM hardness level, delineating the SCHAZ.

4. Discussion

The results obtained in this study revealed important insights regarding the mechanical and microstructural performance of welded joints in UHH-Q&T steels using ASS filler metal. The dilution coefficient remained relatively stable across different welding conditions, which is consistent with previous findings indicating that dilution is predominantly governed by welding current. However, even under consistent dilution levels (51–60%), the interaction between the filler and base metal compositions contributed to the formation of complex phase structures in the FZ, particularly near the weld interface, where the so-called “white phase” region was observed.

The dilution rate plays a central role in determining the final chemical composition of the weld metal, particularly in dissimilar joints, where the interaction between austenitic filler and martensitic base material affects the formation of phases during solidification. As shown in studies by El-Hofy et al. (2022), variations in heat input and joint geometry led to dilution levels ranging from 16 to 35%, shifting the microstructure from austenitic-ferritic to predominantly martensitic structures, consistent with the predictions of the Schaeffler diagram. Similar effects were reported by Shanmugasundar et al. (2023), where dilution altered the balance between retained austenite and martensite in the fusion zone, impacting mechanical performance and hardness distribution. These findings corroborate the significance of dilution as a predictive parameter for metallurgical transformations and weldability in dissimilar combinations [34, 35].

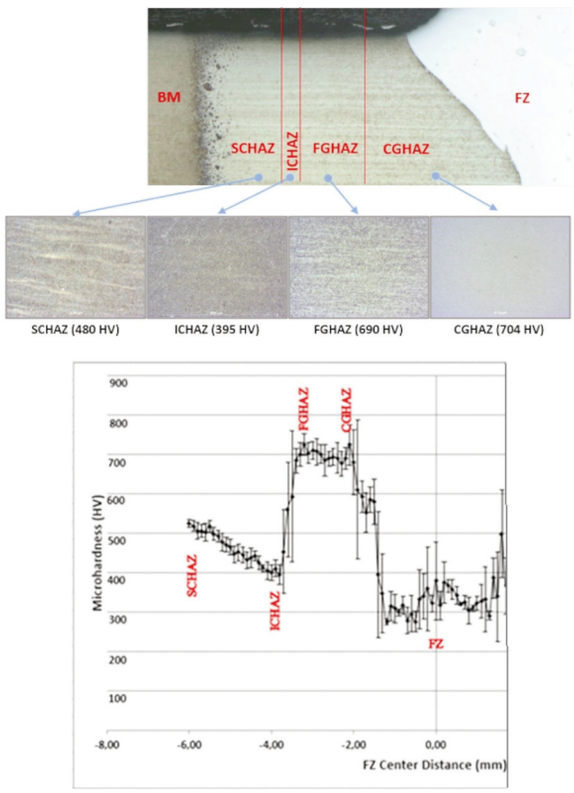

Figure 9. *The microstructures of the HAZ subzones with their corresponding microhardness*

The microstructural composition indicated by the Schaeffler diagram, showing austenitic and martensitic phases, was confirmed by optical and SEM analyses. These results align with the predicted structural zones, where higher dilution values shifted the composition closer to the martensite-austenite boundary, reinforcing the diagram’s applicability for weld microstructure prediction in dissimilar joints. Specifically, joints with $\delta > 57\%$ presented a visibly wider white phase at the fusion boundary, consistent with higher martensitic content.

The microhardness distributions for different parameter sets (Table 2) exhibited slight variations, particularly in the CGHAZ and ICHAZ regions. Notably, shorter stick-out distances produced higher hardness peaks in the CGHAZ, likely due to a more focused heat input and steeper thermal gradients. This behavior was consistent with the finer martensitic structures observed near the fusion line. Conversely, increased welding speed tended to narrow the softened zone and reduce peak CGHAZ hardness, suggesting a moderation in thermal influence across the HAZ.

A key aspect of this study was the evaluation of hardness profiles across the heat-affected zone (HAZ), where four distinct subzones were identified. The coarse-grained HAZ (CGHAZ) reached values up

to 730 HV, while the intercritical HAZ (ICHAZ) experienced softening to around 395 HV. Notably, the softened region presented a narrow width of approximately 0.4 mm. This is a relevant observation since military specifications such as MIL-DTL-46100E tolerate localized softening as long as the overall structural and ballistic integrity is preserved [1].

The softening zone (ICHAZ), although characterized by a significant drop in hardness (395 HV), exhibited an average width of approximately 0.4 mm. According to MIL-DTL-46100E standards, which tolerate localized softening provided that minimum hardness thresholds and ballistic integrity are preserved, this narrow band is unlikely to compromise structural or ballistic performance [1]. The limited extent of the softening zone suggests favorable thermal management during welding.

Although no direct ballistic tests were conducted, the combination of high hardness in the CGHAZ and limited softening suggests that the welded joints may meet ballistic performance requirements. This inference is supported by recent literature reporting that similar hardness ranges and HAZ morphologies effectively resisted 7.62 mm armor-piercing projectiles when appropriate filler metals were employed and thermal cycles were controlled (Subramani et al., 2021; Wei et al., 2024; Ertek et al., 2025). These comparisons validate the use of mechanical and microstructural indicators to anticipate ballistic behavior, especially in preliminary assessments of new welding procedures [36-38].

In summary, the stable dilution values observed, along with favorable hardness profiles and controlled softening, suggest that the welding procedure adopted in this study is well-suited for structural and possibly ballistic applications involving UHH-Q&T steels.

5. Conclusions

This study demonstrated that dissimilar welded joints composed of UHH-Q&T armor steel and austenitic stainless steel filler (ER307) can exhibit favorable microstructural and mechanical characteristics under controlled welding conditions. The key findings are:

Dilution values were stable (51–60%) across variations in welding speed and electrode extension, indicating process robustness;

The CGHAZ maintained hardness values exceeding 675 HV, while the softened ICHAZ was restricted to a narrow band (~0.4 mm), suggesting strong thermal resilience;

Microstructural continuity, with the preservation of martensitic features and absence of brittle intermetallic phases, was confirmed throughout the transition zones.

Although direct projectile resistance tests were not conducted, the correlation with established ballistic benchmarks provides a strong indication that the welding parameters employed here yield joints with structural integrity suitable for defense applications.

These results reinforce the relevance of microstructural engineering and hardness mapping as predictive tools for ballistic performance and highlight the potential of ASS fillers for joining armor-grade steels without sacrificing functional resilience. Future work should focus on confirming these inferences through full-scale ballistic evaluation.

Acknowledgments

The authors would like to thank SSAB Special Steels for providing the base material and Scanning Electron Microscopy Laboratories of the Materials Engineering Section of the Military Institute of Engineering (IME) and the Materials Characterization Laboratory (LACAM) of the Federal University of Para (UFPA) for providing testing and microstructural characterization facilities for this work.

Author Contributions

Charles Hudson Martins de Vasconcelos: Methodology, Validation, Visualization, Writing – original draft; Naiara Vieira Le Sénéchal: Validation, Writing – original draft; Cristhian Ricardo Loayza Loayza: Investigation, Testing; Ademir Ângelo Castro Filho; Investigation, Testing; Eduardo de Magalhães Braga: Writing-Review, Funding acquisition, Formal analysis; Andersan dos Santos Paula: Writing-Review, Over all supervision; Ricardo Pondé Weber: Over all supervision.

Data availability

The data used to support the findings of this study are available from the corresponding author upon request.

Conflict of interest

The authors declare that they have no known competing financial interests or personal relationships that could have appeared to influence the work reported in this paper.

References

[1] U.S. Military Specification MIL-DTL-46100E (MR), Armor Plate, Steel, Wrought, High-Hardness, Army Research Laboratory, AP, MD, 2008.

[2] E. Rapacki, K. Frank, B. Leavy, M. Keele, J. Prifti, Armor steel hardness: Influence on kinetic energy penetration, Proc. 15th International Symposium on Ballistics, Jerusalem, Israel, 1995.

[3] Z.G. Balalan, F. Sarsilmaz, O. Ekinci, Mechanical properties and fatigue behavior of CO_2 laser beam welded armor steel joints, Materials Testing, 62(7) (2020) 689–697. https://doi.org/10.3139/120.111534

[4] L.S. Kim, K.J. Son, Y.S. Yang, P.K.D.V.Yaragada, Sensitivity analysis for process parameters in GMA welding processes using a factorial design method, International Journal of Machine Tools and Manufacture, 43(8) (2003) 763–769. https://doi.org/10.1016/S0890-6955(03)00054-3

[5] L.S. Kim, J.S. Son, J.Y. Kim, I.G. Kim, O.S. Kim, A study on relationship between process variables and bead penetration for robotic CO_2 arc welding, Journal of Materials Processing Technology, 136(1–3) (2003) 139–145. https://doi.org/10.1016/S0924-0136(02)01126-3

[6] R.S.Chandel, Mathematical modeling of gas metal arc weld features, Proc. 4th International Conference on Modeling of Casting and Welding Processes, Palm Coast, FL, 1988, pp. 109–120.

[7] J. Raveendra, R.S. Parmar, Mathematical models to predict weld bead geometry for flux cored arc welding, Metals Construction, 19(2) (1987) 31R–35R.

[8] Z. Zhang, X. Huang, P. Yao, J. Xue, A new method for weld dilution calculation through chemical composition analysis, Metals, 11(131) (2021) 1–10. https://doi.org/10.3390/met11010131

[9] Z. Lin, W. Ya, V.V. Subramanian, C. Goulas, B. di Castri, M.J.M. Hermans, B. Pathiraj, Deposition of Stellite 6 alloy on steel substrates using wire and arc additive manufacturing, International Journal of Advanced Manufacturing Technology, 111(1–2) (2020) 411–426. https://doi.org/10.1007/s00170-020-06116-w

[10] S. Nweze, J. Achebo, The use of fuzzy logic in predicting percentage dilution of weld during TIG welding process, Materials Sciences and Applications, 10(5) (2019) 406–422. https://doi.org/10.4236/msa.2019.105030

[11] M. Aghakhani, E. Mehrdad, E. Hayati, Parametric optimization of gas metal arc welding process by Taguchi method on weld dilution, International Journal of Modeling and Optimization, 1(3) (2011) 216–220. https://doi.org/10.22214/ijraset.2017.9095

[12] Y.L. Sun, G. Obasi, C.J. Hamelin, A.N. Vasileiou, T.F. Flint, J. Balakrishnan, M.C. Smith, J.A. Francis, Effects of dilution on alloy content and microstructure in multi-pass steel welds, Journal of Materials Processing Technology, 265 (2019) 71–86. https://doi.org/10.1016/j.jmatprotec.2018.09.037

[13] SSAB, Armox Welding Recommendations, SSAB, Sweden, 2001, 2 p.

[14] M.A. Morsy, R. El Hebeary, Weldability of armor steel, Proc. 72nd IIW Annual Assembly and International Conference, 7–12 July 2019, pp. 2–10.

[15] G. Magudeeswaran, V. Balasubramanian, G.M. Reddy, Metallurgical characteristics of armour steel welded joints used for combat vehicle construction, Defence Technology, 14(5) (2018) 590–606.

[16] A. Saxena, S.P. Dwivedi, S. Sharma, V.S. Srivastava, A comparative numerical analysis on the effect of welding consumables on the ballistic resistance of SMAW joints of armor steel, Applied Sciences, 11(3629) (2021). https://doi.org/10.3390/app11083629

[17] N.K. Murthy, G.D. Janaki Ram, B.S. Murty, G.M. Reddy, T.J.P. Rao, Carbide-free bainitic weld metal: A new concept in welding of armor steels, Metallurgical and Materials Transactions B, 45 (2014) 2327–2337.

[18] SSAB, Armox Welding Recommendation, SSAB Oxelösund AB, Oxelösund, 2005.

[19] Voestalpine, Böhler Welding Product Catalogue, 2019, pp. 30–360.

[20] ESAB, Welding Filler Metal, in: Databook, 2016.

[21] U.S. Department of Defense, MIL-STD-1185: Manufacturing Process Standard: Welding, High Hardness Armor, 31 Dec. 1979.

[22] A. Popławski, P. Kędzierski, A. Morka, Identification of Armox 500T steel failure properties in the modelling of perforation problems, Materials and Design, 190 (2020) 108536. https://doi.org/10.1016/j.matdes.2020.108536

[23] D.M. Robledo, J.A.S. Gómez, J.E.G. Barrada, Development of a welding procedure for MIL A 46100 armor steel joints using gas metal arc welding, Dyna, 78(168) (2011) 65–71.

[24] American Welding Society, AWS A5.9/A5.9M: Specification for bare stainless steel welding electrodes and rods, Miami, 2012, 46 p.

[25] P.V. Marques, P.J. Modenesi, Some handy equations for welding, Soldagem e Inspeção, 19(1) (2014) 91–102.

[26] P.J. Modenesi, P.V. Marques, D.B. Santos, Introduction to welding metallurgy, UFMG, Belo Horizonte, 2012, 209 p.

[27] ASTM E45-18a, Standard test methods for determining the inclusion content of steel, ASTM International, 2018, 20 p.

[28] ASTM E2142-08(2015), Standard test methods for rating and classifying inclusions in steel using the scanning electron microscope, ASTM International, 2015, 14 p.

[29] ASTM E384-11, Standard test method for Knoop and Vickers hardness of materials, ASTM International, 2011, 43 p.

[30] T. Kannan, N. Murugun, Effect of flux cored arc welding process parameters on duplex stainless steel clad quality, Journal of Materials Processing Technology, 176 (2006) 230–239. https://doi.org/10.1016/j.jmatprotec.2006.03.157

[31] J.U. Ohwoekevwo, A. Ozigagun, J.I. Achebo, K.O. Obahiagbon, Prediction of percentage dilution in AISI 1020 low carbon steel welds produced from TIG welding, Journal of Applied Sciences and Environmental Management, 27(5) (2023) 979–984. https://doi.org/10.4314/jasem.v27i5.14

[32] A.L. Schaeffler, Constitution diagram for stainless steel weld metal, Metal Progress, 56(11) (1949) 680–680B.

[33] N. Bailey, Factors influencing weldability, in: weldability of ferritic steels, Abington Publishing, Cambridge, UK, 1994, pp. 1–44.

[34] H. El-Hofy, M. El-Bakry, W. El-Garaihy, A. Nofal, Effect of dilution and joint configuration on microstructure and mechanical properties of dissimilar welded joints between high-strength steel and stainless steel, Materials Today Communications, 31 (2022) 103478. https://doi.org/10.1016/j.mtcomm.2022.103478

[35] K. Shanmugasundar, R. Singh, M. Vasudevan,

Influence of dilution and post weld heat treatment on microstructure and mechanical properties of dissimilar welds between martensitic and austenitic steels, Journal of Materials Research and Technology, 25 (2023) 1794–1806. https://doi.org/10.1016/j.jmrt.2023.06.159

[36] P. Subramani, A. Sharma, T. Jayakumar, Evaluation of ballistic performance of welded joints in high hardness armor steels, Defence Technology, 17(6) (2021) 1905–1913. https://doi.org/10.1016/j.dt.2021.02.004

[37] Y. Wei, Z. Liu, H. Wang, Y. Li, Influence of welding parameters on hardness and ballistic resistance of ultra-high hardness armor steel welds, Materials Science and Engineering A, 889 (2024) 145652. https://doi.org/10.1016/j.msea.2024.145652

[38] A. Ertek, Y. Kaya, B. Demir, Optimization of fusion welding techniques for enhanced ballistic resistance in ultra-high hardness steels, Journal of Manufacturing Processes, 89 (2025) 339–350. https://doi.org/10.1016/j.jmapro.2025.03.012

UTICAJ PARAMETARA ZAVARIVANJA NA PROCENAT RAZBLAŽENJA I MEHANIČKA SVOJSTVA U ZAVARENIM SPOJEVIMA OKLOPNIH ČELIKA ULTRA-VISOKE TVRDOĆE

Charles Hudson Martins de Vasconcelos [a,c*], Naiara Vieira Le Sénéchal [a], Cristhian Ricardo Loayza Loayza [b], Ademir Ângelo Castro Filho [b], Eduardo de Magalhães Braga [b], Andersan dos Santos Paula [a], Ricardo Pondé Weber [a]

[a] Vojni institut za inženjerstvo - IME, Odeljenje za nauku o materijalima i inženjerstvo, Rio de Žaneiro, Brazil

[b] Federalni univerzitet Para - UFPA, Odsek za mašinsko inženjerstvo, Belem, Brazil

[c] Centar za obuku Admiral Braz de Agiar - SIABA, Belem, Brazil

Apstrakt

Ova studija ispituje uticaj parametara zavarivanja elektrolučnim postupkom u zaštitnoj atmosferi (GMAW) — konkretno brzine zavarivanja i izbočenje elektrode — na razblaživanje i mehanička svojstva zavarenih spojeva koji se sastoje od ultra-visoko tvrdog kaljenog i otpuštenog (UHH-Q&T) oklopnog čelika i filera od austenitnog nerđajućeg čelika. Metodologija optimizacije korišćena je za postavljanje konstantnih parametara, uključujući prečnik žice, protok gasa, napon zavarivanja i brzinu dodavanja žice, na osnovu mogućnosti opreme. Eksperimentalni pokušaji varirali su brzinu zavarivanja i izbočenje elektrode uz održavanje konstantne struje putem kontrole induktivnosti. Iako su parametri zavarivanja uticali na površine istopljenog osnovnog i dodatnog metala, procenat razblaživanja ostao je nepromenjen. Validirana je korelacija između razblaživanja i struje zavarivanja. Mikrostrukturne i mehaničke analize potvrdile su konzistentno ponašanje zavarenih spojeva pod ispitivanim uslovima.

Ključne reči: *Čelik ultra-visoke tvrdoće; GMAW; Razblaživanje; Zona uticaja toplote; Mehanička svojstva*